Pacific Northwest
NATIONAL LABORATORY

PNNL-33873

Casting and Characterization of U-50Zr

January 2022

Prepared By:
Zach Huber and Elise Conte

With Contributions by:
Curt Lavender
James Fornof
Eric Shaber
Andrey Mushakov
Jon Johnson
Aaron Totemeier
Forrest Heller
Aaron Nicholas
Benjamin Lund
Matthew Olszta
Dana Arbova
Lucas Sweet
Robert Gomez
Scott Swenson
Sergey Sinkov

U.S. DEPARTMENT OF ENERGY

Prepared for Lightbridge Corp

DISCLAIMER

PACIFIC NORTHWEST NATIONAL LABORATORY
operated by
BATTELLE
for the
UNITED STATES DEPARTMENT OF ENERGY
under Contract DE-AC05-76RL01830

Printed in the United States of America

Available to DOE and DOE contractors from the Office of Scientific and Technical Information,
P.O. Box 62, Oak Ridge, TN 37831-0062
www.osti.gov
ph: (865) 576-8401
fax: (865) 576-5728
email: reports@osti.gov

Available to the public from the National Technical Information Service
5301 Shawnee Rd., Alexandria, VA 22312
ph: (800) 553-NTIS (6847)
or (703) 605-6000
email: info@ntis.gov
Online ordering: http://www.ntis.gov

PNNL-33873

Casting and Characterization of U-50Zr

January 2022

Prepared By:
Zach Huber and Elise Conte

With Contributions by:

Curt Lavender	Aaron Totemeier	Dana Arbova
James Fornof	Forrest Heller	Lucas Sweet
Eric Shaber	Aaron Nicholas	Robert Gomez
Andrey Mushakov	Benjamin Lund	Scott Swenson
Margaret Lund	Matthew Olszta	Sergey Sinkov

Prepared for
Lightbridge Corp.

Pacific Northwest National Laboratory
Richland, Washington 99354

Abstract

Uranium alloyed with approximately 50 wt% zirconium (U-50Zr) is proposed as a water-cooled reactor nuclear fuel by Lightbridge Corporation (LTBR). One possible method for making the U-50Zr alloy is to arc-melt master alloys and then remelt in a vacuum induction melter (VIM) to consolidate the material and then cast the material into an intermediate shape. After casting, the material can be formed into a desired fuel shape. The work discussed in this report resulted from a joint effort between LTBR and Pacific Northwest National Laboratory (PNNL) to investigate a 500g – 1kg scale casting process to produce a U-50Zr alloy in the desired δ-UZr_2 phase and characterize the impurities and microstructure that result from the casting process.

Master alloys were fabricated in an arc melter, then five castings were carried out in a VIM with multiple inert coating and crucible materials to find an appropriate combination. Both ZrO_2 and graphite crucibles were used along with different combinations of Y_2O_3, $CaZrO_3$, and TiC coatings to identify which would contain the molten metal with the least reaction. On each casting, the C, O, N, H impurities were analyzed as well as the phase by x-ray diffraction and microstructure.

Of the five castings, two resulted in majority of δ-UZr_2 phase-pure material with acceptably low impurity levels. The two most successful castings utilized a graphite crucible with a TiC undercoating and a Y_2O_3 overcoat. The O and N levels were below 1000 ppm and the C content was variable but did not result in measurable carbide formation. The highest success casting resulted in an average of 282 ppm C, 567 ppm O, 217 ppm N and 79 ppm H. This casting's crucible and inert coating material was repeated with slightly different casting parameters and resulted in higher C numbers but similar phase identification. The differences between each casting are discussed and recommendations are made for future experiments.

Acknowledgments

The authors wish to acknowledge the excellent technical support provided by Pacific Northwest National Laboratory's Paul MacFarlan, Matthew Athon, and K. Marie McCoy. Numerous valuable conversations on technical challenges were discussed with these individuals. Ali Zbib provided programmatic support throughout the project.

Additionally, this project was a joint effort with Lightbridge Corporation. This partnership added invaluable insights, discussion, and direction to this work throughout.

Acronyms and Abbreviations

BSE	backscatter electron
CRADA	Cooperative Research and Development Agreement
DI	deionized
DOE	Department of Energy
EDS	energy dispersive spectrometry
EMS	electromagnetic stirring
GAIN	Gateway for Accelerated Innovation in Nuclear
LTBR	Lightbridge Corporation
NDIR	non-dispersive infrared
SEM	scanning electron microscopy
U-50Zr	Uranium alloyed with 50 wt% Zirconium
UHP	Ultra high purity
VIM	Vacuum Induction Melter

Contents

Abstract ii
Acknowledgments iii
Acronyms and Abbreviations iv
1.0 Introduction 1
2.0 Casting and Characterization Methodology 2
2.1 Arc Melting 2
2.2 Vacuum Induction Melting 2
2.3 Analysis 3
2.3.1 C/O/N/H 3
2.3.2 XRD 4
2.3.3 SEM 4
3.0 Results 5
3.1 Arc Melt Master Alloy 5
3.2 VIM Casting 1 6
3.3 VIM Casting 2 9
3.4 VIM Casting 3 13
3.5 VIM Casting 4 16
3.6 VIM Casting 5 20
4.0 Discussion 24
5.0 Recommendations and Future Work 27
6.0 Conclusions 28
7.0 References 29

Figures

Figure 1: Arc melted U-50Zr master alloy buttons. 5
Figure 2: VC-1 billet before cleaning.. 7
Figure 3: VC-1 Sampling diagram.. 7
Figure 4: XRD results from VC-1. 8
Figure 5: Micrographs of VC-1. 9
Figure 6: VC-2 billet before cleaning. 10
Figure 7: VC-2 and VC-3 cut diagram.. 11
Figure 8: XRD results from VC-2 12
Figure 9: Micrographs of VC-2. 13
Figure 10: VC-3 billet before cleaning. 14
Figure 11: XRD results from VC-3. 15
Figure 12: Micrographs of VC-3 16
Figure 13: VC-4 billet before cleaning. 17
Figure 14: VC-4 and VC-5 cut diagram. 18
Figure 15: XRD results from VC-4 19
Figure 16: Micrographs of VC-4. 20
Figure 17: VC-5 billet before cleaning. 21
Figure 18: VC-5 cut diagram. 22
Figure 19: XRD results from VC-5 23
Figure 20: Visualization of the C, O, N, H across all castings. 26

Tables

Table 1: Casting parameters for each VIM casting. 3
Table 2: Average impurities of the arc melted master alloys and feedstock 5
Table 3: C, O, N, H analyses for VC-1. 7
Table 4: C, O, N, H analyses for VC-2 11
Table 5: C, O, N, H analyses for VC-3. 14
Table 6: C, O, N, H analyses for VC-4 18
Table 7: C, O, N, H analyses for VC-5 22

1.0 Introduction

Uranium alloyed with ~50 wt% zirconium (U-50Zr) is a proposed water-cooled reactor nuclear fuel by Lightbridge Corporation (LTBR). A proposed method for making the U-50Zr alloy is to arc-melt master alloys and then remelt in a vacuum induction melter (VIM) to consolidate the material prior to casting into an intermediate shape. After casting, the material will be formed into a desired fuel shape. The work discussed in this report investigates a casting process to produce the U-50Zr alloy in the desired phase (δ-UZr_2) and characterizes the impurities and microstructure that result from the casting process.

Pacific Northwest National Laboratory in collaboration with LTBR obtained funding through the Department of Energy's Gateway for Accelerated Innovation in Nuclear (DOE-GAIN) program and established a Cooperative Research and Development Agreement (CRADA). The overarching goal of this project was to identify an appropriate casting method (i.e., crucible and coating combination) that results in an acceptable impurity concentration in the as-cast ingot. This report summarizes the efforts of that work.

Uranium and Zr are well known to be highly reactive metals and must be handled carefully to reduce their molten interactions with air and crucible materials. A common problem is the α-phase stabilization of the two metals by O and N impurities (Rough et al. 1956, Janney 2018). This stabilized phase is undesirable in nuclear reactor fuels (Hofman et al. 1990). Additionally, carbon impurities in the alloy can form UC and ZrC phases that are hard and brittle. These carbides are prone to crack formation during subsequent forming operations, so they must be minimized. Due to these issues, proper mold, crucible, and inert coating selection is essential.

Little literature on the casting of U-50Zr is published. The authors have found limited relevant data on the mold, crucible, or inert coatings for containing molten U-50Zr. There is only one documented instance (McCoy 2020) where a U-50Zr casting was successful, but the impurity contents were not well characterized. Samples of U-50Zr are usually prepared by arc melting in an inert Ar atmosphere and limited to the 20-30 gram range (Basak 2010, Basak 2011, Bagchi 2014, Bagchi 2014, Khanolkar 2021). Apart from arc melting, other methods of producing Zr-rich U-Zr alloys are rarely reported. In one instance, a method used 34g of U-50Zr in a Y_2O_3 to melt-cast. Precipitates from the crucible as well as C- and O-stabilized Zr precipitates were observed in the microstructure (Ahn 2014, Irukuvarghula 2016). U-60.5Zr has been produced through powder metallurgy (Lee 2008) but U and Zr powders are more prone to absorbing O than the U rod and Zr sponge typically used in casting (Bagchi 2014). U-10Zr has been cast in Y_2O_3-coated graphite crucibles but a ZrC reaction layer was formed at the melt-crucible interface and ZrC precipitates were found in the matrix. These results suggest that above 1500°C, the Y_2O_3 coating reacts with the graphite crucible and C migrates through the coating into the melt (Ha 2021). U-Zr alloys containing 2, 5, 7, and 10 wt% Zr were cast in Y_2O_3-coated graphite crucibles at 100°C above the liquidus temperature and analysis showed increasing C content with increasing wt% Zr (Basak 2009). As casting temperature increases with wt% Zr, this implies a Y_2O_3 coating alone will not be robust enough to cast U-50Zr in a graphite crucible without exceeding acceptable impurity levels.

The lack of relevant and substantial literature on more than gram-scale casting, processing, and chemistry of U-50Zr has prompted the present work to investigate the inert coatings and the crucible materials that are needed to contain the molten metal and minimize impurity reactions within the melt. After casting the alloy, characterization was carried out on phase, impurities, and microstructure to further inform processing methodologies for the alloy.

2.0 Casting and Characterization Methodology

2.1 Arc Melting

Uranium chunks and Zr crystal bar was used as the starting material. The U feedstock was used as ~25g rectangles and etched prior to being alloyed. The etching process used an 8M nitric acid bath for 10 minutes followed by a deionized (DI) water rinse and ethanol to dry. The Zr bar was cut into 10-40g pieces and was rinsed in ethanol prior to being placed in the arc-melting chamber. Within half an hour of cleaning, the material was placed in the chamber and under vacuum. Typically, buttons were 60-80g each. The U and Zr were weighed to be within 1g of each other.

The U and Zr metals were alloyed using an Edmund Buehler MAM-1 arc-melter in a static ultra-high purity (UHP) argon atmosphere on a water-cooled Cu crucible. The melting chamber was evacuated with a turbomolecular vacuum pump and backfilled three times using UHP argon to atmospheric pressure. The UHP argon was run through a gas drier and Matheson gas purifier intended to remove oxygen. During the final evacuation, the chamber was evacuated to a minimum of 10^{-3} mbar. The metals were melted together at the maximum achievable current (140 amps) and flipped seven times for a total of eight melts. Prior to the first melting and after each flip of the button, a separate piece of Zr metal was melted to getter any remaining contaminants. The Zr getter was kept in a separate well inside of the arc-melter.

Between each button made, the chamber was cleaned with ethanol and soft paper wipes. After every 15 buttons made, the copper crucible was sanded to remove a noticeable black buildup and smooth the surface. After sanding, to remove grit and prepare the surface for use, it was rinsed in DI water and ethanol. The first melting cycle after cleaning was pure Zr that was not reused for button production. To monitor button quality, C, O, N, and H impurities were measured after every five buttons produced.

2.2 Vacuum Induction Melting

The castings were made using an Indutherm VTC 200V Ti tilt-pour VIM operating at approximately 17 kHz frequency. The induction heater can achieve a maximum power of 15 kW. The VIM was modified to allow for larger molds and the introduction of resistance mold heaters and thermocouples by adding a bolt-on extension to the mold side of the system.

The VIM is equipped with roughing/backing pumps and a turbomolecular pump capable of reaching an ultimate vacuum of 10^{-5} mbar. The VIM induction coil has 10 turns of copper piping, an outer diameter of 3.25", an inner diameter of 2.75", a height of 2.75", and is cooled internally by flowing chilled glycol. The temperature of the melt is measured by an optical pyrometer with a minimum readable temperature of 800°C and a maximum temperature of 2100°C.

The graphite crucible used was made from isomolded graphite obtained from GraphiteStore.com in grade GR001CC. The graphite was machined at Pacific Northwest National Laboratory to an outer diameter of 2.05”, inner diameter of 1.73”, and an inner opening length of 5.25”. The zirconia crucible was magnesia stabilized and purchased from Zircoa Inc. and had a 2" inner diameter with an inner opening length of 5.125". The graphite crucible had a wall thickness of 0.16” and the zirconia crucible had a wall thickness of 0.2".

The graphite crucible castings utilized a TiC underlayer and an inert Y_2O_3 overcoat purchased from ZYP Coatings. Above 1500°C, the Y_2O_3 is susceptible to carbothermic reduction in the presence of graphite (Ha 2021). This results in loss of the inert integrity and C, Y, and oxide contamination. It is believed that the same reduction does not happen with Y_2O_3 and TiC due to the higher chemical stability of TiC. The TiC coating was applied by airbrush three times on warm graphite (50-75°C) followed by three coatings with Y_2O_3. Casting numbers and parameters for each casting are listed in Table 1. For VC-1, VC-2, and VC-3, the coating was baked between applications for 1 hour at 100°C in air. After realizing that this may not be adequate for removing the water carrier, VC-4 and VC-5 utilized 300°C vacuum bakeouts for a minimum of 1 hour between all applications and an overnight final bakeout. The higher temperature and vacuum atmosphere improved the probability that all water of hydration was fully removed from the coating.

The ZrO_2 crucible utilized a Y_2O_3-$CaZrO_3$ (60:40 mol% ratio; ZYP Coatings) coating that is marketed as better suited for applications with ceramic crucibles and highly reactive molten materials. The coating was applied three times with an airbrush to a warm ZrO_2 crucible and baked at 100°C between each coating for a minimum of one hour. No overnight curing procedure was done.

Each of the five castings had slightly varying conditions in an attempt to establish the most successful method to pursue going forward. The casting parameters for each are listed in Table 1. For the final three castings, before loading the charged crucible, a vacuum leak rate check was completed. The leak-up rate was measured as <15 mtorr/min. Before power was applied to the induction coil, the system was evacuated for 3 minutes and purged with argon for all castings. This was repeated three times for a total of four evacuations. The VIM was set to run at 6-9 kW until maximum temperature was reached, after which the power was modulated by the VIM system to maintain the hold temperature.

Table 1: Casting parameters for each VIM casting.

Casting Number	Crucible Material	Coating Material and Number of Coats	Total Mass of Buttons (g)	Target Hold Temperature (°C)	Time When Visibly Molten	Hold Time After Molten
VC-1	Graphite	3x Y_2O_3 over 3x TiC	1,023	1,900	6 min 9 sec	5 min 0 sec
VC-2	ZrO_2	3x Y_2O_3-$CaZrO_3$	1,010	1,900	7 min 51 sec	1 min 0 sec
VC-3	ZrO_2	3x Y_2O_3-$CaZrO_3$	992	1,875	10 min 50 sec	2 min 0 sec
VC-4	Graphite	3x Y_2O_3 over 3x TiC	607	1,875	8 min 0 sec	2 min 0 sec
VC-5	Graphite	3x Y_2O_3 over 3x TiC	598	1,875	6 min 30 sec	7 min 11 sec

2.3 Analysis

2.3.1 C/O/N/H

The C/O/N/H impurities were determined for every five master alloy buttons produced and multiple locations in each of the five castings. The C impurity was measured by a LECO C230 Carbon by Combustion Determinator instrument. The instrument was calibrated before taking the measurement using a single point steel calibration standard obtained from LECO and three

blank runs. Calibration checks were run every five samples. Chunks used for C analysis weighed between 0.3 g and 0.6 g and were loaded into a ceramic crucible after letting an isopropanol rinse fully dry. The native oxide layer was not removed and the pieces were prepared in air.

For the O/N/H impurity measurements, an inert gas fusion method was used with a LECO model ONH836. A minimum of three graphite crucible with tin flux blank standards were run to measure the instrument background. A set of three certified reference standards were run to generate a calibration curve encompassing a wide range of possible values (O: 36–1160 ppm; N: 70–557 ppm; H: 3–99 ppm). Each sample was inserted into a nickel basket and placed in the crucible with a small amount of graphite powder (approximately 0.05 g) and tin flux. The sample and crucible were then heated in an impulse furnace to release the analyte gases. The carbon monoxide and carbon dioxide generated by the O in the sample was measured by non-dispersive infrared (NDIR) cells. The H present in the sample was oxidized to form H_2O and measured by the NDIR cells. The N present in the sample was measured using a thermal conductivity detector.

2.3.2 XRD

The cut samples of U-50Zr were mounted on glass slides using putty and sealed with Kapton film as a radiological containment control. X-ray diffraction (XRD) data were collected on the metals using a Rigaku Ultima IV diffractometer equipped with a Cu sealed tube X-ray source (Cu Ka 1.5406 Å) and a linear position sensitive detector. Data was collected between 5° and 100° 2θ using a 10 mm divergence slit, a 0.5° incident slit, 5° primary and secondary Soller slits, and a Ni foil filter to reduce contributions from Kβ. The data were collected in 0.02° count binning steps at a 2° per minute scan rate. Phase identification and quantification was performed using the Rietveld refinement within the TOPAS v6 software package.

2.3.3 SEM

Microstructural and microchemical characterization of the vacuum cast U-50Zr alloys was achieved using variable accelerating voltage JEOL 7600 scanning electron microscopy (SEM) in backscatter electron (BSE) mode as well as using energy dispersive spectrometry (EDS). A JEOL inline, low angle BSE detector was used to probe the Z contrast of each alloy and an Oxford 170 mm^2 X-max EDS detector was used for chemical analysis. In order to investigate the nanoscale microstructure of the alloys, short working distances (~4.5 mm) at an accelerating voltage of 7.5 kV were utilized to minimize the interaction volume to differentiate smaller phases from the bulk microstructure. Accelerating voltages of 9 kV at a working distance of 15 mm were used to collect the U-M and Zr-L edges for chemical detection. Data collection and analysis was performed using the Oxford AZtec program and the montaging module for collection of large area maps to demonstrate possible homogeneity of the microstructures and microchemistry.

3.0 Results

3.1 Arc Melt Master Alloy

Each of the five castings utilized arc melted U-50Zr master alloy buttons as shown in Figure 1. The first three castings (VC-1, VC-2, VC-3) utilized approximately 15 buttons to make the one kg casting charge. The fourth and fifth casting (VC-4 and VC-5) utilized approximately 10 buttons to make a 600g charge. The C, O, N, and H content was measured on every fifth button to ensure consistent conditions and no degradation of the arc melting crucible or components. Additionally, as can be seen in Figure 1, the first button made was more heavily sampled to investigate if impurity gradients exist across one button. The measured values for the analyzed buttons are shown in Table 2**Error! Reference source not found.**. The table also includes the starting feedstock levels of the U and Zr metals used. In general, the arc melted buttons picked up little to no contamination of the measured impurities and impurities were not location dependent. It appears that O impurities were slightly decreased by arc melting. It is possible that free O was released upon the first melting and then reacted with the separate Zr getter that's melted between each flip of the button.

Figure 1: Arc melted U-50Zr master alloy buttons. Some buttons were cut for analysis. The top left button was heavily sampled to investigate if impurity gradients existed across a button. Each button is 60-80g before cutting.

Table 2: Average impurities of the arc melted master alloys and the starting U and Zr feedstock. The number following the ± is one standard deviation and the number of samples for each analysis is indicated in parentheses.

Sample	Average Carbon, ppm	Average Oxygen, ppm	Average Nitrogen, ppm	Average Hydrogen, ppm
Arc Melt U-50Zr	48 ± 16 (N=19)	84 ± 46 (N=26)	26 ± 49 (N=26)	15 ± 5 (N=26)
U Feedstock	56 ± 21 (N=5)	72 ± 7 (N=4)	0 (N=4)	11 ± 1 (N=4)
Zr Feedstock	45 ± 11 (N=11)	180 ± 80 (N=8)	0 (N=8)	23 ± 11 (N=8)

3.2 VIM Casting 1

The first casting (VC-1) utilized graphite as the crucible material, which has been successfully used in the past to cast U-50Zr (McCoy 2020) and many other U alloys (Huber, McCoy, et. al. 2021, Huber, Athon, et. al. 2021). In the present investigation, an additional TiC undercoating was used to reduce reactions between the Y_2O_3 coating and the graphite crucible. Above 1,500°C, there is a known carbothermic reduction of the coating resulting in carbon uptake of the molten metals (Ha 2021). The TiC coating is more stable in the casting environment and able to prevent the carbothermic reduction of the inert Y_2O_3 coating. Additionally, instead of a vacuum environment where in-leakage of air is possible, this casting was done in one atmosphere of UHP-Ar. With additional heating produced through convection (as opposed to just radiation in vacuum environments), high temperatures at the lid of the VIM and on the induction coil's PTFE passthroughs penetrations were observed. This resulted in failures of o-ring seals and the PTFE. For the following castings, a vacuum environment was chosen to mitigate these risks.

Due to previous successful pouring of the castings (McCoy 2020), an attempt was made to pour the first two castings. The melt was not successfully poured from the crucible to the mold. It appeared that the top of the melt did not move at all, and no molten metal was transferred. It is unknown why this was not successful.

Upon removal of the billet from the VIM, an interaction was observed between the graphite crucible walls and the billet. The graphite crucible had to be broken to remove the stuck billet. A picture of the billet can be seen in Figure 2. Multiple issues were identified and attempted to be fixed. The first issue was during loading buttons, the potential to scratch the inert coating off the wall. This was fixed in subsequent castings by using vacuum tweezers to lower the buttons carefully into the crucible. Secondly, the coating is a water-based coating and was baked out at 100°C for one hour between and after all the coatings. There is potential that not all water of hydration was released during these bakeouts. Later castings mitigated this risk by baking at 300°C in a vacuum environment.

The billet was sectioned into top, middle, and bottom samples, as shown in Figure 3, and then analyzed for major impurities, phases, and microstructure. The results of the analyses can be seen in Table 3, Figure 4, and Figure 5. There were variable impurities with some samples experiencing severe C, O, and N uptakes. In general, the middle of the billet had substantially less contamination. This could be attributed to interactions with environment for the melt's top and interactions with the large surface area of the crucible bottom.

Phase data collected by XRD showed the presence of ZrC and α -Zr with the majority of the samples being delta phase, UZr_2. Due to strong orientation dependence and large grain sizes, the quantification (in wt%) of fits are approximate. For the top sample, there was 73% UZr_2, 17% ZrC, and 10% α-Zr. For the middle sample, there was 78% UZr_2 and 22% ZrC. For the bottom sample, there was 98% UZr_2 and 2% ZrC. The presence of α-Zr in the top indicates reaction with O or N resulting in the stabilization of α-phases.

Micrographs in Figure 5 clearly show a much larger presence of carbide impurities in the top sample when compared against the bottom, which aligns well with the phase results. The carbides appear finely dispersed throughout the top sample as small black inclusions. In the bottom sample, the longer, high aspect ratio inclusions are alpha stabilized phases rather than carbides. In the top sample, the presence of the α-Zr stabilized phase was not clearly seen in the EDS scan or overview image.

Figure 2: VC-1 billet before cleaning. A) The billet side view. B) The opposite side view with an arrow indicating where the crucible and melt reacted. C) The billet bottom contacting the crucible bottom. D) The billet top which was exposed to the VIM environment.

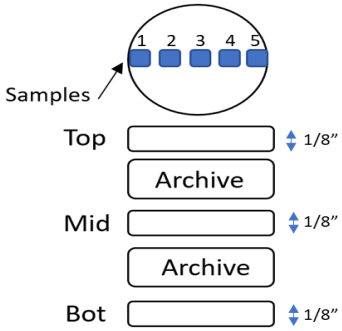

Figure 3: VC-1 Sampling diagram. Samples 1-5 were cut from each the Top, Middle, and Bottom sections shown.

Table 3: C,O,N,H data measured for VC-1. Middle 5 was not measured for C.

Sample Name	Carbon, ppm	Oxygen, ppm	Nitrogen, ppm	Hydrogen, ppm
VC-1 Top 1	1,471	2,000	4,162	58
VC-1 Top 2	1,216	2,153	4,319	64
VC-1 Top 3	1,498	5,188	8,703	79
VC-1 Top 4	1,243	2,362	4,637	73
VC-1 Top 5	1,479	2,039	3,897	59
VC-1 Middle 1	839	991	1,574	31
VC-1 Middle 2	626	1,040	1,667	29
VC-1 Middle 3	929	903	1,503	35
VC-1 Middle 4	603	1,262	2,105	37
VC-1 Middle 5	-	1,073	1,789	29
VC-1 Bottom 1	1,428	2,655	4,269	38
VC-1 Bottom 2	927	6,673	10,931	44
VC-1 Bottom 3	3,519	1,607	1,180	35
VC-1 Bottom 4	964	1,651	2,756	35
VC-1 Bottom 5	2,534	182	287	48
VC-1 Average	**1,377**	**2,119**	**3,585**	**46**

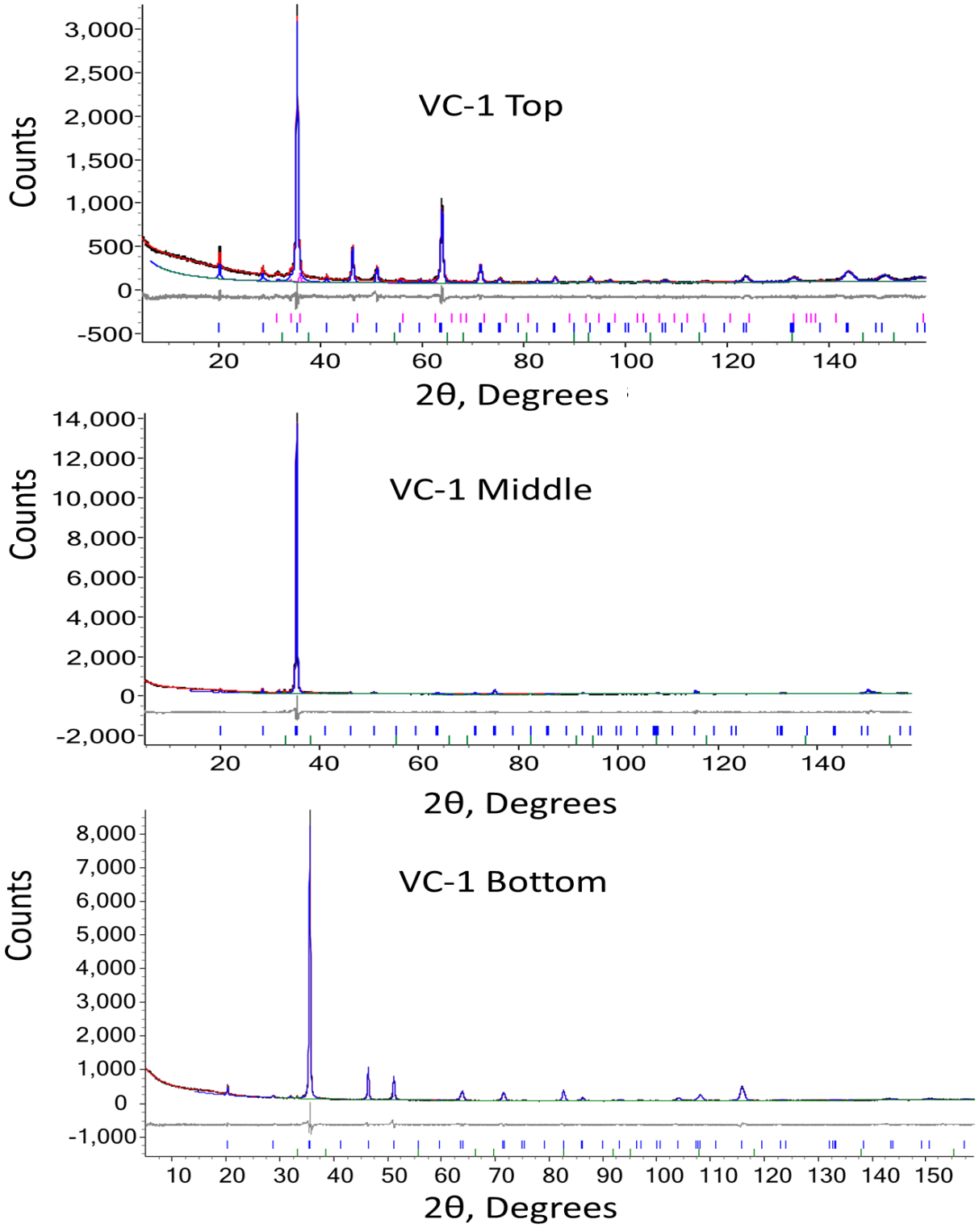

Figure 4: XRD results from VC-1 Top, Middle, and Bottom sections is shown by the black line. The delta phase, UZr_2, is fit with a blue line, ZrC with green, and α-Zr with pink. The overall fit is in red and the difference between fit and observed data is in grey.

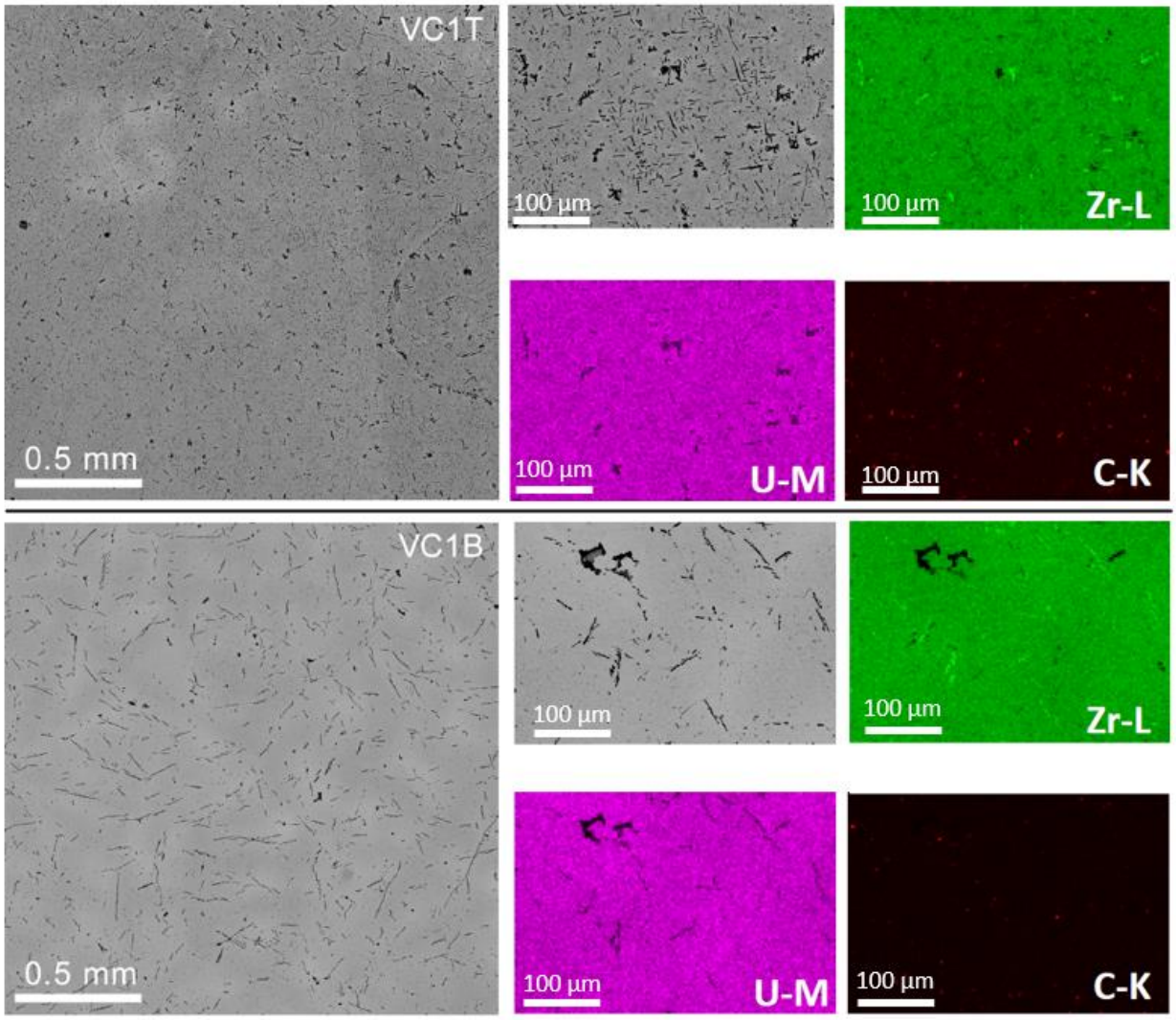

Figure 5: Micrographs of VC-1 Top sample (VC1T) and Bottom sample (VC1B). The leftmost image is an overview of the sample, and the right images show representative EDS scans of the microstructure.

3.3 VIM Casting 2

VIM Casting 2 was made using a ZrO_2 crucible instead of graphite crucible to decrease the C and O melt contamination that is frequently associated with the use of graphite. Zirconia has successfully been used in the past for casting other U alloys (Huber, McCoy, et. al. 2021, Huber, Athon, et. al 2021) and resulted in high yield, low impurity castings. Additionally, it was thought to be beneficial to use a crucible that is nonconducting which can enable electromagnetic stirring (EMS) and therefore promote melt homogeneity (Huber, Athon, et. al. 2021). This melt was attempted to be tilt poured into a mold like VC-1 but was again unsuccessful.

Upon removal of the crucible from the VIM, reaction of the billet, inert coating, and crucible was observed. The crucible had cracked and had to be broken off the billet to completely remove it. A picture of the billet post-casting and before cleaning can be seen in Figure 6.

The billet was sectioned in half longitudinally, then portions cut for sampling. The full sampling plan and cuts can be seen in Figure 7. The impurity analyses can be seen in Table 4. Minor C increases were observed in the casting. Despite the low C levels that are desirable, the O and N levels were exceedingly high in all the samples analyzed. Post casting, it was found that the VIM had a vacuum leak in the PTFE passthrough likely due to VC-1 being in an Ar environment. It was hypothesized that the significant O and N contamination in the sample analyses was due to the air in leakage. After casting VC-2, the passthrough penetrations were replaced and vacuum leak rates were frequently monitored.

As expected with very high levels of O and N impurities, significant α-phase stabilization was observed in the phase identification from each section as shown in Figure 8. The top section had 22% UZr_2, 17% α -Zr, and 61% α-U. The middle-top section had 6%, 83%, and 12% respectively. The middle-bottom section had 28% Uzr_2 and 72% α-Zr. The bottom section had 32% Uzr_2, 20% α-Zr, and 48% α-U.

Micrographs of the top and bottom sections are shown in Figure 9. The images are saturated with the high aspect ratio inclusions indicative of the alpha stabilized phases. This agrees well with the phase identification and impurity analyses. In the EDS, it becomes abundantly clear that the inclusions are stabilized α-Zr as they are devoid of U content. Then in the matrix directly next to the stabilized α-Zr, EDS shows increased U content as seen by the brighter pink coloration. In the top micrograph, the thick black regions with white centers are voids in the sample and not part of the U-50Zr microstructure.

Figure 6: VC-2 billet before cleaning. A) billet side view. Just below (to the right) of where the brown halo is seen is the top of the continuous billet. Above that (to the left) of the halo is a very thin layer that was adhered to the crucible walls but not part of the continuous billet. B) The opposite side view of the billet. C) Top view of the billet which was exposed to the VIM atmosphere. The thin layer adhered to the crucible can be easily seen extending past the top of the billet. D) The bottom of the billet which was in contact with the ZrO_2 crucible

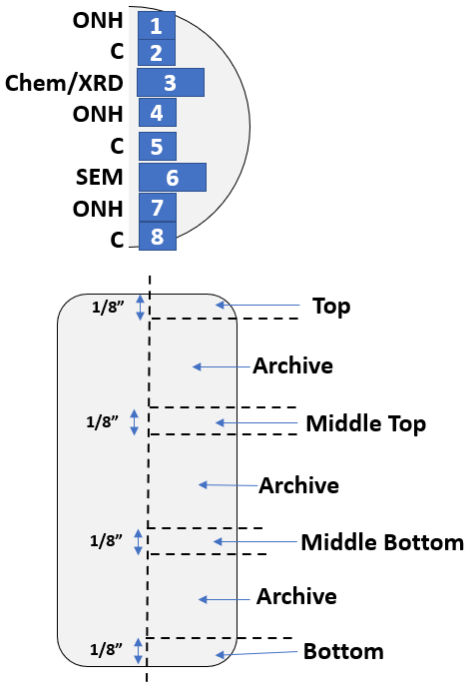

Figure 7: VC-2 and VC-3 cut diagram. The dotted black lines are where cuts were made. The top image is the location where the samples are taken from and their identifying number.

Table 4: C, O, N, H analyses for VC-2. The average of each analysis across the whole billet is shown in the last column.

Sample Name	Carbon, ppm	Sample Name	Oxygen, ppm	Nitrogen, ppm	Hydrogen, ppm
VC-2 Top 2	152	VC-2 Top 1	7,524	13,101	16
VC-2 Top 5	79	VC-2 Top 4	6,212	10,676	12
VC-2 Top 8	190	VC-2 Top 7	2,797	4,922	55
VC-2 Middle Top 2	83	VC-2 Middle Top 1	8,594	15,147	17
VC-2 Middle Top 5	70	VC-2 Middle Top 4	5,178	9,154	12
VC-2 Middle Top 8	102	VC-2 Middle Top 7	6,124	10,740	20
VC-2 Middle Bottom 2	63	VC-2 Middle Bottom 1	5,910	10,514	17
VC-2 Middle Bottom 5	176	VC-2 Middle Bottom 4	1,788	3,268	34
VC-2 Middle Bottom 8	110	VC-2 Middle Bottom 7	5,899	10,595	12
VC-2 Bottom 2	78	VC-2 Bottom 1	7,875	14,342	19
VC-2 Bottom 5	85	VC-2 Bottom 4	5,381	9,590	26
VC-2 Bottom 8	245	VC-2 Bottom 7	5,343	9,459	22
VC-2 Average	**119**	**VC-2 Average**	**5,719**	**10,126**	**22**

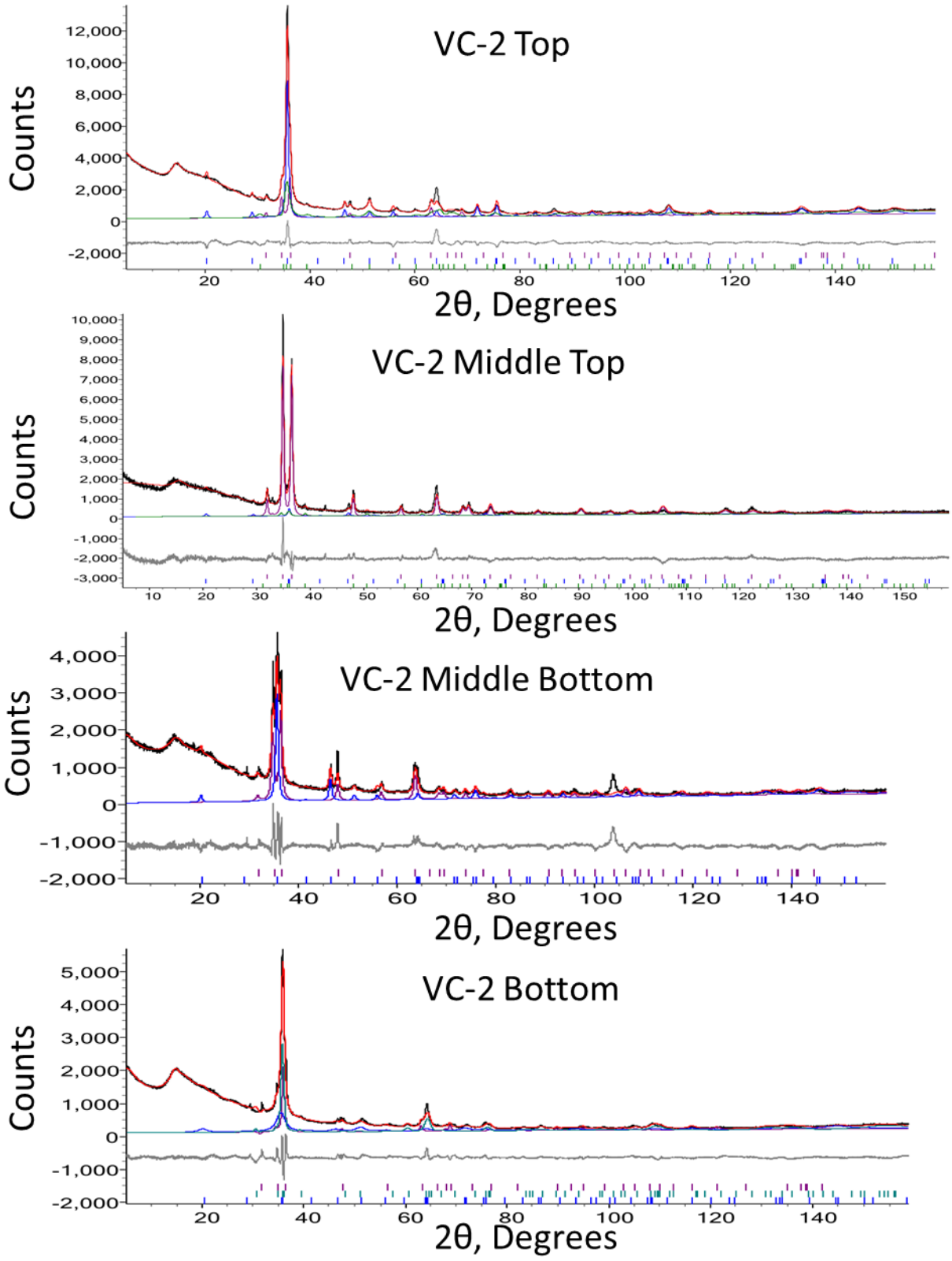

Figure 8: XRD results from VC-2 samples are shown by the black line. The delta phase, Uzr_2, is fit with a blue line, α-Zr with green, and α-U metal with green. The overall fit is in red and the difference between fit and observed data is in grey.

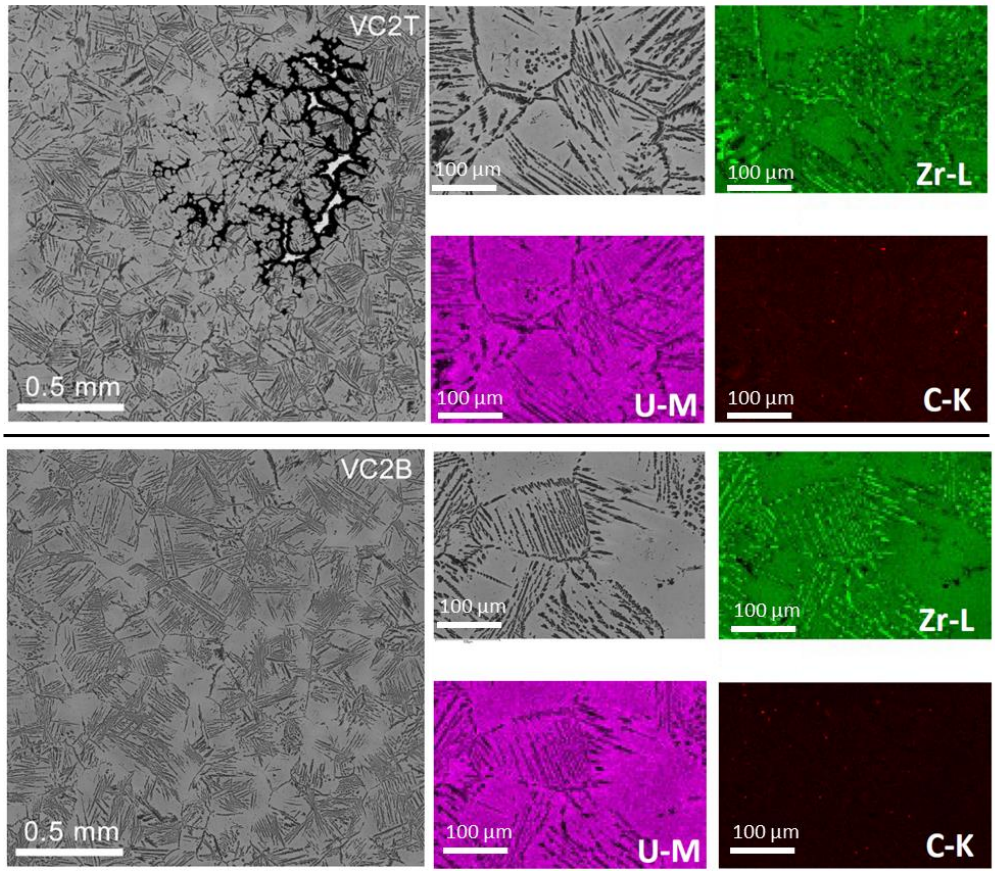

Figure 9: Micrographs of VC-2 Top and Bottom. The leftmost image is an overview of the sample, and the right images show representative EDS scans of the microstructure.

3.4 VIM Casting 3

The VC-2 crucible and inert coating conditions were repeated for VC-3 after the vacuum leak was fixed. Due to the lack of success of pouring VC-1 and VC-2, it was decided to just melt VC-3 and cool in place. Upon removal of the crucible from the VIM, it was again discovered that the billet had to be broken out of the crucible. Pictures of the VC-3 billet can be seen in Figure 10.

VC-3 used the same cutting diagram as VC-2. The impurity analyses can be seen in Table 5. Despite the vacuum leak rate being checked beforehand and verifying low leak up rates before casting, VC-3 had considerable O and N contamination. As expected with the elevated levels of O and N impurities, significant α-phase stabilization was observed in the phase identification from each section as shown in Figure 11. The top section had 35% UZr_2, 31% α -Zr, and 34% α-U. The middle-top section had 38%, 36%, and 25% respectively. The middle-bottom section had 53% UZr_2 and 10% α-Zr, 20% α-U, and 17% ZrC. The bottom section was not analyzed by XRD. The occurrence of ZrC at such high quantities was unexpected and does not agree well with the measured C contents. Considering such high O and N contamination, the XRD of the bottom sample and the occurrence of substantial ZrC was not further investigated.

As expected with significant alpha stabilization due to O and N impurities, the micrographs in Figure 12 look very similar to those in VC-2. The high aspect ratio Zr precipitates are even more numerous due to the increased contamination. During EDS, a C coating instead of Au coating

was used hence the difference in the EDS from previous samples. The C rich areas (especially in the bottom sample) are associated with voids in the metal sample where the epoxy filled in during metallurgical sample preparation. These are not related to the microstructure of the material.

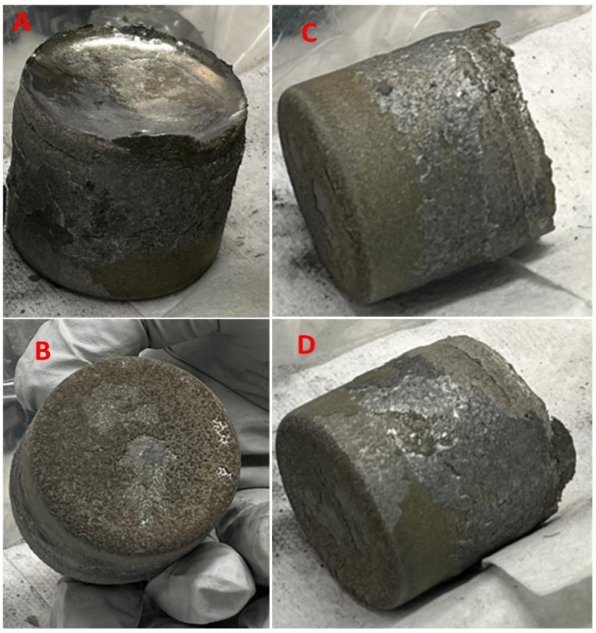

Figure 10: VC-3 billet. A) Top of the billet. B) Bottom side of the billet. C) Side of the billet showing interaction with the crucible coating. D) Opposite side of the billet showing interaction with the crucible coating.

Table 5: C, O, N, H analyses for VC-3. The average of each analysis across the whole billet is shown in the last column.

Sample Name	Carbon, ppm	Sample Name	Oxygen, ppm	Nitrogen, ppm	Hydrogen, ppm
VC-3 Top 2	102	VC-3 Top 1	7,441	13,596	8
VC-3 Top 5	141	VC-3 Top 4	9,668	17,874	16
VC-3 Top 8	102	VC-3 Top 7	7,330	13,553	7
VC-3 Middle Top 2	136	VC-3 Middle Top 1	9,899	17,986	3
VC-3 Middle Top 5	121	VC-3 Middle Top 4	8,381	15,186	1
VC-3 Middle Top 8	176	VC-3 Middle Top 7	8,538	15,471	2
VC-3 Middle Bottom 2	136	VC-3 Middle Bottom 1	10,954	20,526	11
VC-3 Middle Bottom 5	480	VC-3 Middle Bottom 4	9,679	18,556	112
VC-3 Middle Bottom 8	206	VC-3 Middle Bottom 7	7,822	15,380	11
VC-3 Bottom 2	450	VC-3 Bottom 1	11,718	23,402	67
VC-3 Bottom 5	648	VC-3 Bottom 4	14,948	29,698	47
VC-3 Bottom 8	282	VC-3 Bottom 7	13,093	25,912	21
VC-3 Average	**248**	**VC-3 Average**	**9,956**	**18,928**	**26**

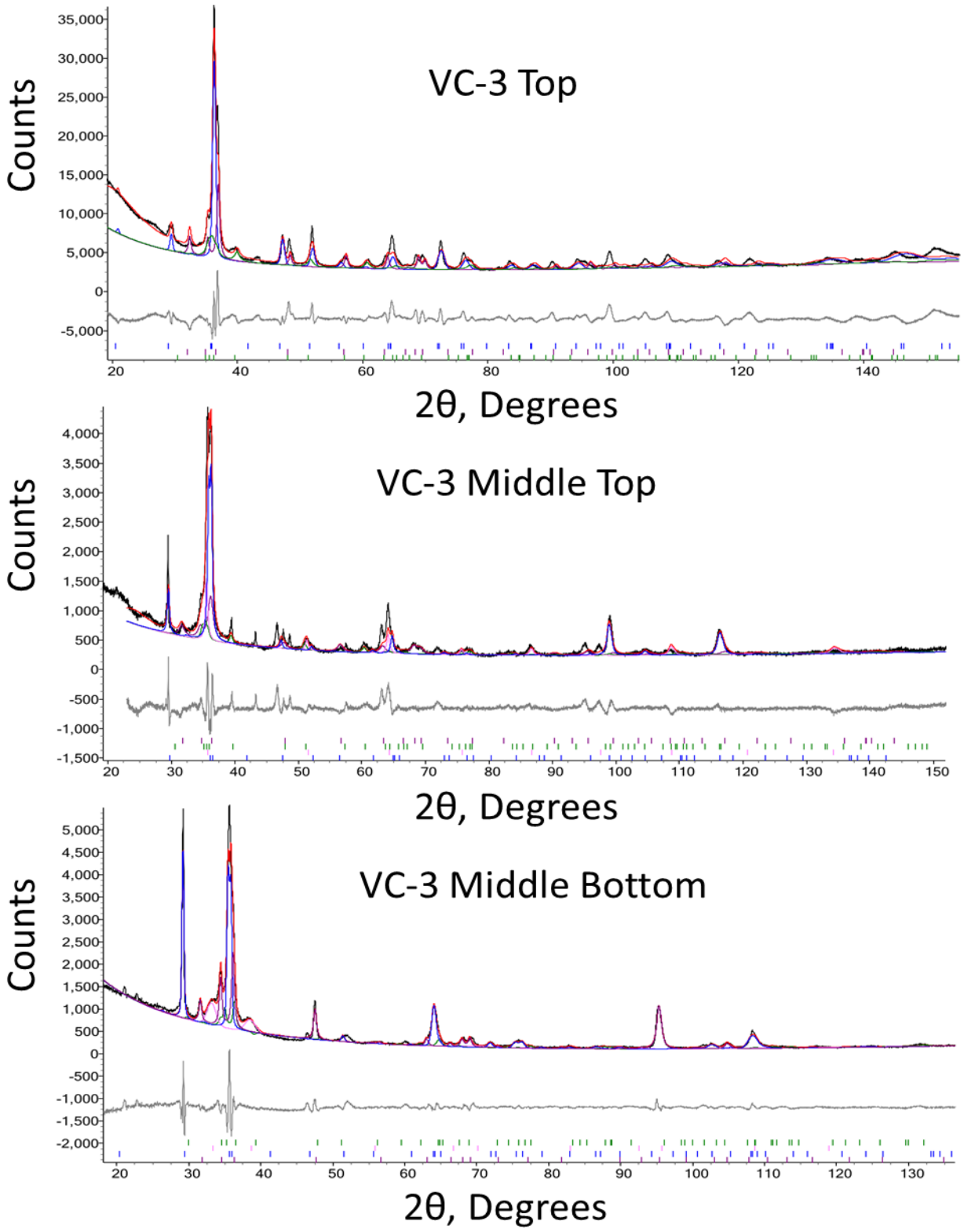

Figure 11: XRD results from VC-3 samples are shown by the black line. The delta phase, UZr_2, is fit with a blue line, α-Zr with purple, α-U with green, and ZrC with pink. The overall fit is in red and the difference between fit and observed data is in grey.

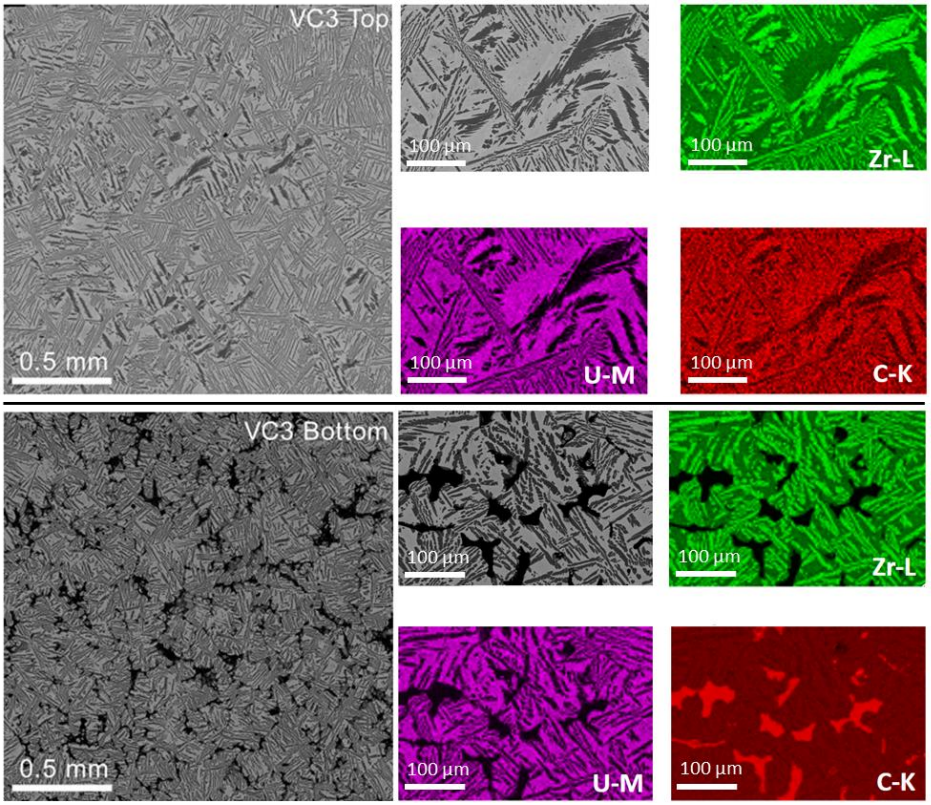

Figure 12: Micrographs of VC-3 Top and Bottom. The leftmost image is an overview of the sample, and the right images show representative EDS scans of the microstructure.

3.5 VIM Casting 4

Due to the severe O and N contamination when using the ZrO_2 crucible and Y_2O_3-$CaZrO_3$ mixed coating, it was decided to go back to a baseline process using TiC and Y_2O_3 coating on graphite. After the clear failure of the coating in VC-1 (indicated by the reaction of the billet and crucible), the coating method was changed to minimize potential for coating spallation due to retained water in the inert coating layers. Further details of the preparation can be found in Section 2.0. After casting, the billet was able to be removed easily from the crucible. The billet can be seen in Figure 13. There was a clear bulbous region on the top of the casting. It appeared this might be an unmelted master alloy button though it seemed unlikely at the time. Additionally, the top of the casting had a brown layer indicating a thin layer of oxidation. Upon further investigation, that layer was less than 15 µm thick. Below that was the shiny silver appearance typical of U-50Zr.

In an effort to conserve as much of the VC-4 casting as possible for potential future forming and heat treating studies, minimal sampling was done. The bulbous region was removed to investigate whether it was an unmelted button, and a bottom section was characterized as well like in VC-2 and VC-3 sampling. A sampling diagram can be seen in Figure 14 and the results of the C, O, N, H analyses are listed in Table 6. Results of VC-4 indicated low C, O, N, H contamination present in the material. All values were low enough to avoid appreciable alpha stabilization and problematic carbide formation and were considered well below the contamination limits that are optimal for this alloy.

The phase identification for VC-4 can be seen in Figure 15. In the top sample, the phase identification mainly identifies α-Zr with a single small peak (~28°) indicating the presence of ZrO_2. The bottom sample has mainly UZr_2 phase but low angle peaks were absent suggesting the presence of small amounts of the gamma BCC U-50Zr phase. The top sample region analyzed by XRD was just below the brown oxide layer on top, which could be why mainly α-Zr is identified. The presence of mainly UZr_2 and potentially untransformed gamma phase is in close agreement with the impurity results. The microscopy for both top and bottom samples, shown in Figure 16, also agrees well with the phase identification on the bottom and the lack of high impurity levels. A few Zr rich precipitates can be seen, but overall, the images show a well distributed, C-free mix of U and Zr. In the micrographs no difference in microstructure was observed in the bulbous region. Figure 17 shows an example of the region that appears to be a button separate from the whole.

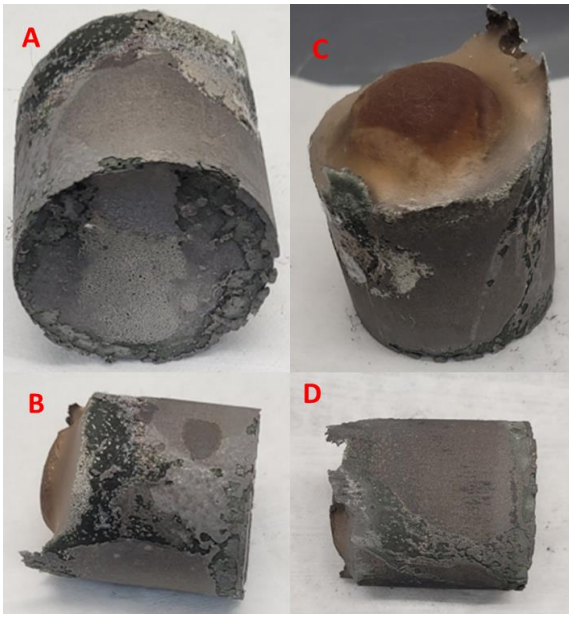

Figure 13: VC-4 billet before cleaning. A) Bottom of the billet. B) Longitudinal side of the billet. C) Top of the billet showing a bulbous region resembling a master alloy U-50Zr button. D) Opposite side of the billet than that shown in B).

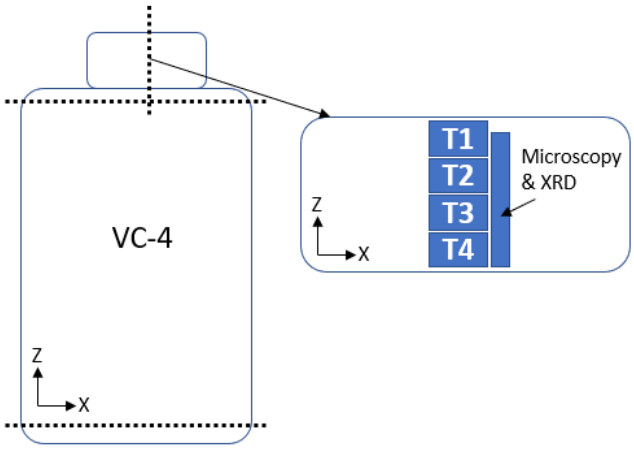

Figure 14: VC-4 and VC-5 cut diagram. The dotted black lines are where cuts were made. The top section was sampled as shown in the right from the bulbous region (drawn with a box on top). The bottom section was sampled like that of VC-2 and VC-3 (shown in Figure 7).

Table 6: C, O, N, H analyses for VC-4. The average of each analysis across the whole billet is shown in the last column.

Sample Name	Carbon, ppm	Sample Name	Oxygen, ppm	Nitrogen, ppm	Hydrogen, ppm
VC-4 T1	345	VC-4 T2	222	343	38
VC-4 T3	216	VC-4 T4	800	400	304
VC-4 Bottom 2	282	VC-4 Bottom 1	619	105	18
VC-4 Bottom 5	287	VC-4 Bottom 4	629	107	20
VC-4 Bottom 8	282	VC-4 Bottom 7	566	131	13
VC-4 Average	**282**	**VC-4 Average**	**567**	**217**	**79**

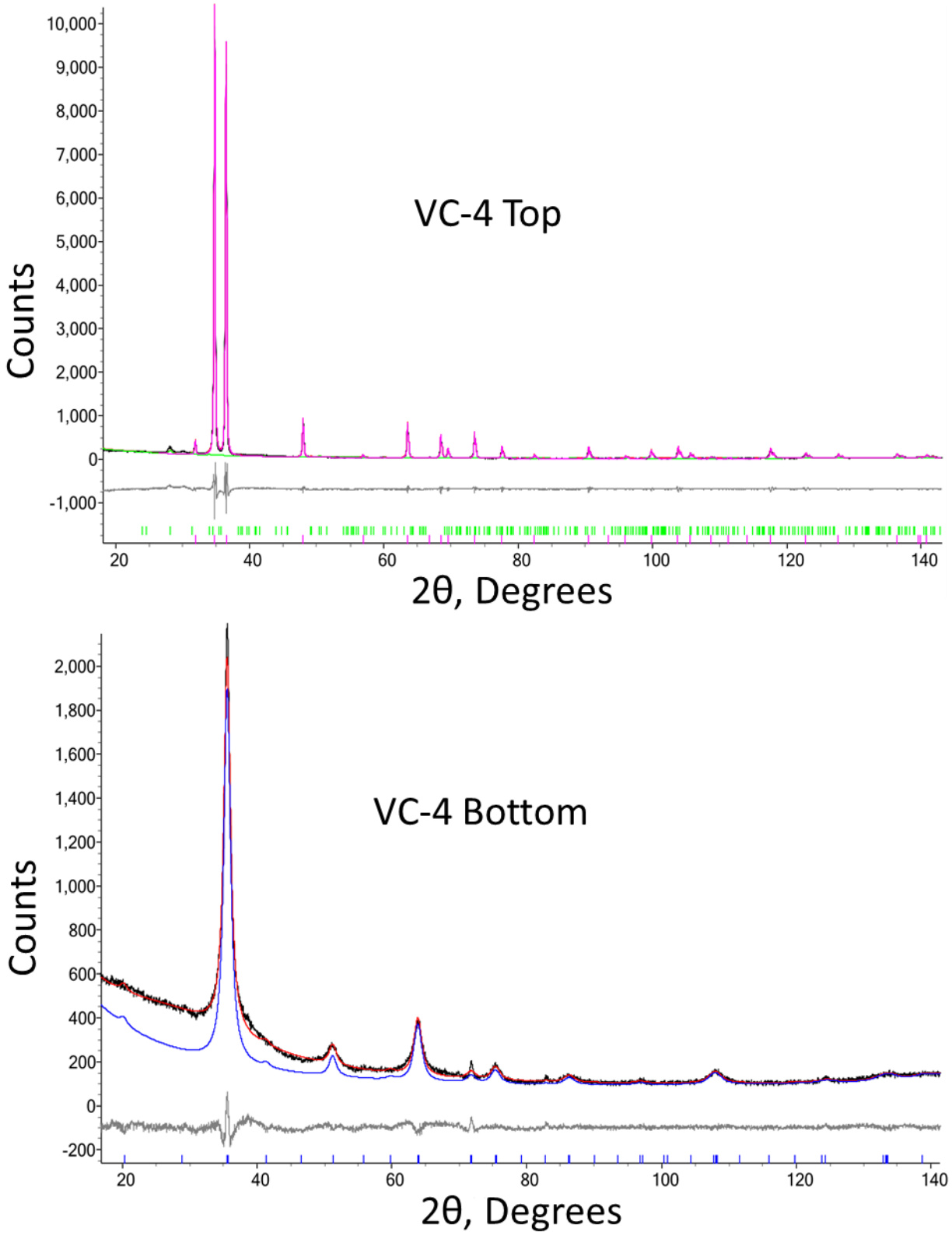

Figure 15: XRD results from VC-4 top and bottom samples are shown by the black line. The delta phase, UZr_2, is fit with a blue line, and α-Zr with a pink line. The overall fit is in red and the difference between fit and observed data is in grey.

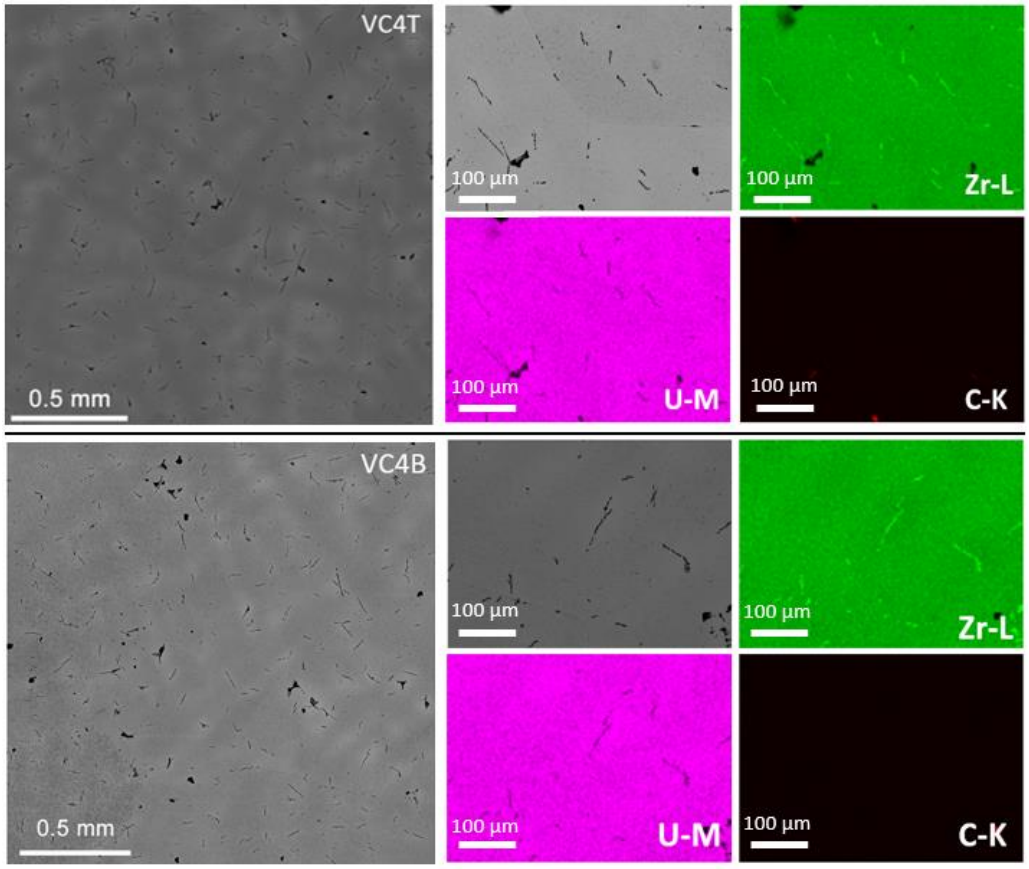

Figure 16: Micrographs of VC-4 Top and Bottom. The leftmost image is an overview of the sample, and the right images show representative EDS scans of the microstructure.

3.6 VIM Casting 5

After the successful casting with low impurity levels and high delta phase purity, VC-4 was repeated but with a slightly increased hold time in an attempt to ameliorate the potential unmelted button that was seen in the bulbous region at the top of VC-4. During casting, there appeared to be a bright but unmelted button while watching the melt through the VIM window. The hold time was increased to wait for it to integrate into the full melt below, but no obvious change was seen for multiple minutes and the choice was made to investigate after pulling the billet from the system. After removal a obvious bulbous region was again seen in the top of the melt. The billet can be seen in Figure 17.

A section through the bulbous region is shown in Figure 17C with an arrow indicating the different contrast region showing where the bulbous region was. Additionally, the thin brown oxide layer was again observed in the top of the billet. No indication of crucible-billet interaction was seen on the sides of the billet. Despite no clear interaction, the billet was stuck inside the graphite crucible and had to be physically removed by breaking the graphite crucible. The billet sides did have higher surface roughness than in VC-4. This is potentially due to reusing the graphite crucible from VC-4.

Initial sampling of the VC-5 billet was done the same as VC-4 where a top and bottom section was cut and analyzed for C, O, N, H impurities and XRD. After finding higher impurities than in VC-4, it was decided to cut a longitudinal section from the billet for impurity analysis to better understand the distribution and confirm if the impurities were indeed higher as indicated by the first top and bottom section analyses. A cut plan for the longitudinal sectioning can be seen in Figure 18 and the initial top and bottom sectioning was the same as shown in Figure 14 for VC-4. The measured values of O and N in the initial sampling was substantially higher as seen in Table 7. This was expected due to the potential interaction of the top of the billet with any potential air inleakage and the bottom of the billet with the surface of the crucible. The second sampling was approximately 0.125" offset away from the extreme ends of the billet and therefore had less interaction with the atmosphere and crucible bottom resulting in lower O and N measured. Despite this, the C content was still elevated and on average significantly higher than in VC-4. The low O and N contamination and high C content indicates the graphite crucible (or TiC coating) interacted with the melt, but minimal air leaked into the vacuum chamber during casting. Additionally, the C content in the bottom section of the billet was much lower than the middle and top sections likely indicating floating of solid carbides occurred as can be expected since they are not molten at these temperatures.

The XRD spectra are presented in Figure 19. The top sample had a majority of α-Zr with a very small amount of UO_2 present. The middle and bottom sample was pure UZr_2. The bottom sample was the expected ordered hexagonal UZr_2 whereas the middle sample appeared to be the disordered UZr_2 phase as evidenced by the lack of certain orientation peaks that were expected and seen in other pure UZr_2 spectra from the other samples analyzed. As with VC-4, the top sample was analyzed very close to the brown oxide layer and therefore the UO_2 and alpha stabilization of Zr make sense. Despite the high levels of C measured in the samples, there is no detectable ZrC or UC. It is unclear what form the elevated C content took.

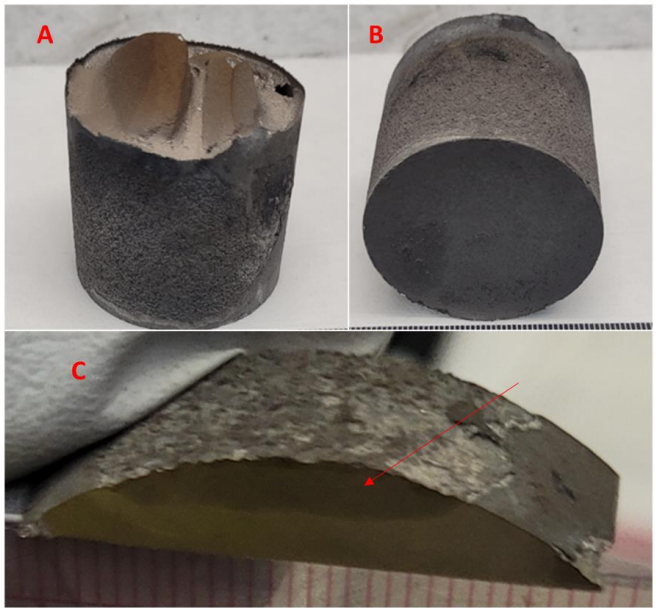

Figure 17: VC-5 billet before cleaning. A) Top of the billet showing the bulbous region B) Bottom of the billet C) Section through the bulbous region showing a different contrast region (highlighted by red arrow) of the potentially unmelted button.

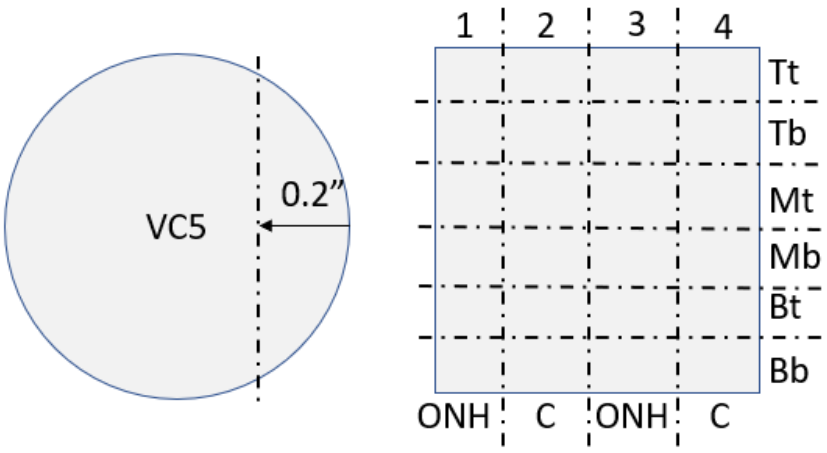

Figure 18: VC-5 cut diagram for the second set of sampling. The left image shows the first cut made longitudinally down the billet 0.2” in from the side. That section was then cut into the 24 samples shown on the right image with each coordinate showing the sample number (1-4) and the location (Tt-Bb). On the bottom is the respective analysis planned for each coordinate number (i.e., all 1’s for ONH and all 2’s for C).

Table 7: C, O, N, H analyses for VC-5. The average of each analysis across the whole billet is shown in the last column. The first five samples are from the initial sectioning shown in Figure 14 and the last 11 samples are from the subsequent sectioning shown in Figure 18. Due to a void, the Tt 2 and Tt 3 samples were too small to analyze.

Sample Name	Carbon, ppm	Sample Name	Oxygen, ppm	Nitrogen, ppm	Hydrogen, ppm
VC-5 T1	431	VC-5 T2	271	30	12
VC-5 T3	83	VC-5 T4	196	28	12
VC-5 Bottom 2	1,958	VC-5 Bottom 1	154	117	20
VC-5 Bottom 8	3,930	VC-5 Bottom 4	1,139	137	27
VC-5 Bottom 5	2,186	VC-5 Bottom 7	62	0	9
VC-5 Tt 4	906	VC-5 Tt 1	251	11	10
VC-5 Tb 2	6,995	VC-5 Tb 1	432	0	20
VC-5 Tb 4	3,577	VC-5 Tb 3	358	13	10
VC-5 Mt 2	1,079	VC-5 Mt 1	349	12	7
VC-5 Mt 4	1,973	VC-5 Mt 3	403	0	12
VC-5 Mb 2	316	VC-5 Mb 1	88	0	13
VC-5 Mb 4	2,802	VC-5 Mb 3	214	4	8
VC-5 Bt 2	281	VC-5 Bt 1	326	4	16
VC-5 Bt 4	711	VC-5 Bt 3	346	7	16
VC-5 Bb 2	284	VC-5 Bb 1	265	0	11
VC-5 Bb 4	289	VC-5 Bb 3	245	6	9
VC-5 Average	**1,737**	**VC-5 Average**	**319**	**23**	**13**

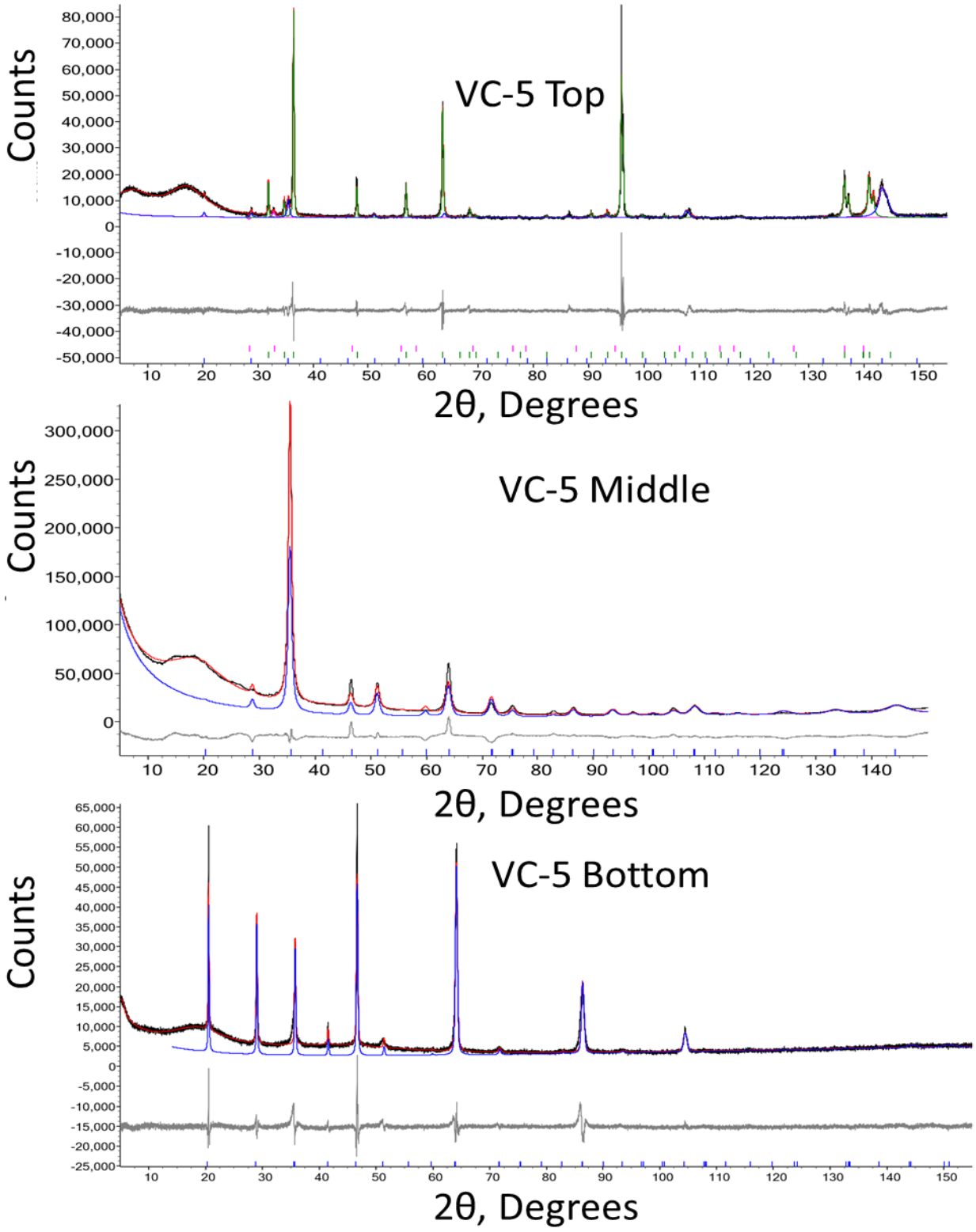

Figure 19: XRD results from VC-5 top and bottom samples are shown by the black line. The delta phase, UZr_2, is fit with a blue line, α-Zr with a green line and UO_2 with a pink line. The overall fit is in red and the difference between fit and observed data is in grey.

4.0 Discussion

The overarching goal of this project was to identify an appropriate casting method that results in low concentration of C, O, N, and H impurities with a secondary goal of obtaining a phase-pure δ-UZr_2 alloy of U-50Zr. While no impurity (C,O,N,H) limits were specified, the aim was to minimize these impurities as elevated levels can detrimentally affect the phase purity and downstream processing. The area of main investigation was the use of crucibles and inert coating material.

The use of graphite crucibles and Y_2O_3 coatings is the industry norm for VIM casting of U alloys. For this reason, it was the baseline process for this study. An alternative TiC undercoating was chosen to prevent adverse reactions identified in previous literature (Ha 2021) as well as the Y_2O_3 carbothermic reduction expected in the conditions needed for casting U-50Zr. No available literature indicates VIM casting of similar quantities of U-50Zr as performed in this work, and the use of a TiC undercoat had not yet been proven effective.

During this work, specifically in the VC-4 casting, it was determined that the use of TiC on graphite crucibles as an undercoat followed by an overcoat of Y_2O_3 works to produce the phase purity and low impurity levels desired. That being said, there were multiple areas of improvement identified between the attempts with VC-1, VC-4, and VC-5. It was identified that water-based coatings must be cured in a vacuum atmosphere at or above 300°C to prevent spallation of the coating and subsequent reaction with the melt. Other methods to cure the coating are possible but were not investigated in this work.

Additionally, the reuse of graphite crucibles, while possible, should be done with careful attention to preserving the crucible surface in the cleaning process. It is believed that the higher surface roughness of the crucible after using it for VC-4 led to the higher carbon contamination in VC-5. The crucible was cleaned using Scotch-Brite pads and water/ethanol after VC-4. This inevitably led to higher surface roughness and therefore higher surface area. The increased roughness makes the application of uniform coatings of TiC and Y_2O_3 more difficult and increases the chance of inert coating failure. A different coating method that produces thicker coatings may increase the life of graphite crucibles. A cleaning method that does not degrade the smooth machined surface of the graphite should also be investigated.

The use of ZrO_2 crucibles, while desirable in many U casting operations, were not successful in this work. In previous work conducted by the authors (McCoy 2020) and in the present work (VC-2 and VC-3), ZrO_2 crucibles did not produce acceptable U-50Zr so the use of these crucibles must be investigated further to determine if they will work. Yttria and $CaZrO_3$-Y_2O_3 mixed coatings resulted in unacceptable O and N contamination in this work. Additionally in this work, EMS was not beneficial because of interactions with air inleakage. It is presumed that the constant stirring allows for the VIM atmosphere-molten metal interface to constantly be broken and mixed into the melt. The high reactivity of the molten metal inleakage of air during vacuum allows for the oxide skin that forms at the top of the melt to incorporate into the molten metal. Without stirring, the oxide skin that forms at the atmosphere-melt interface becomes an impenetrable layer and thus provides a diffusion barrier between air and the molten metal. In air-sensitive, highly reactive melts, the EMS is likely detrimental if any air inleakage is present. Because EMS was used with a ZrO_2 crucible in this study (VC-

2/VC-3), it was impossible to determine if the $CaZrO_3$-Y_2O_3 coating successfully acted as a non-reactive inert coating for molten U-50Zr.

C, O, N impurity trends across samples was of high interest for insight into post-casting machining and forming operations. Figure 20 compares impurity trends for one element across the locations in all castings. The size of each symbol was mapped to the impurity value where the largest symbols represented larger impurity content. Considering that the operating parameters changed for each of the castings, it was not feasible to draw firm conclusions on impurity trends across samples. While consistent casting parameters would have made the trends easier to understand, the aim was to identify a successful approach on variable parameters. Two successful castings (VC-4 and VC-5) were achieved in terms of low O and N impurities and phase purity. Although the C content in VC-5 was elevated, there were no indications of carbide phases in the XRD data. There were no clear impurity trends between all castings from top to bottom nor edge to middle.

The C content in VC-1 and VC-5 were the most elevated of all the castings. It is interesting that VC-4, while also done in graphite, had lower C contamination. This was attributed to the coating effectiveness as discussed above. Between individual castings, trends were evident such as VC-5 having C mostly concentrated in the topmost section and had a decreasing trend down the casting length. This is likely attributable to the longest hold time allowing the carbide impurities a chance to float towards the top of the melt (they are solids at these temperatures). VC-1, VC-2, and VC-3 all had the highest C contamination in the bottom of the sample (difficult to see because of the low values compared to other castings), potentially due to the largest surface area contact at the bottom of the crucible and low hold times preventing carbide floating. Except for these minor trends, the only other trend was the high correlation between O and N contamination, which is consistent with a reaction between air and the molten metal.

A couple of interesting phenomena to note were the seemingly random stabilization of the α-U and α-Zr phases. There appeared to be no correlation as to whether high O or N contamination resulted in one of the α-phases preferentially stabilizing over the others. Additionally, the lack of ZrC or UC phases identified in VC-5 as opposed to the significant carbide phases present in VC-1 was not expected. VC-5 had slightly higher C contents than VC-1, but no carbide phase identified. This could potentially point to the higher O and N contamination in VC-1 playing a role in the formation of identifiable carbide phases.

Overall, it appears as though low C, O, N impurities and phase-pure UZr_2 are possible using the TiC-Y_2O_3 coating method on graphite crucibles when using the appropriate precautions. Further investigation is warranted to understand the role that O and N may play in carbide phase stabilization and whether ZrO_2 crucibles are appropriate for use with this alloy.

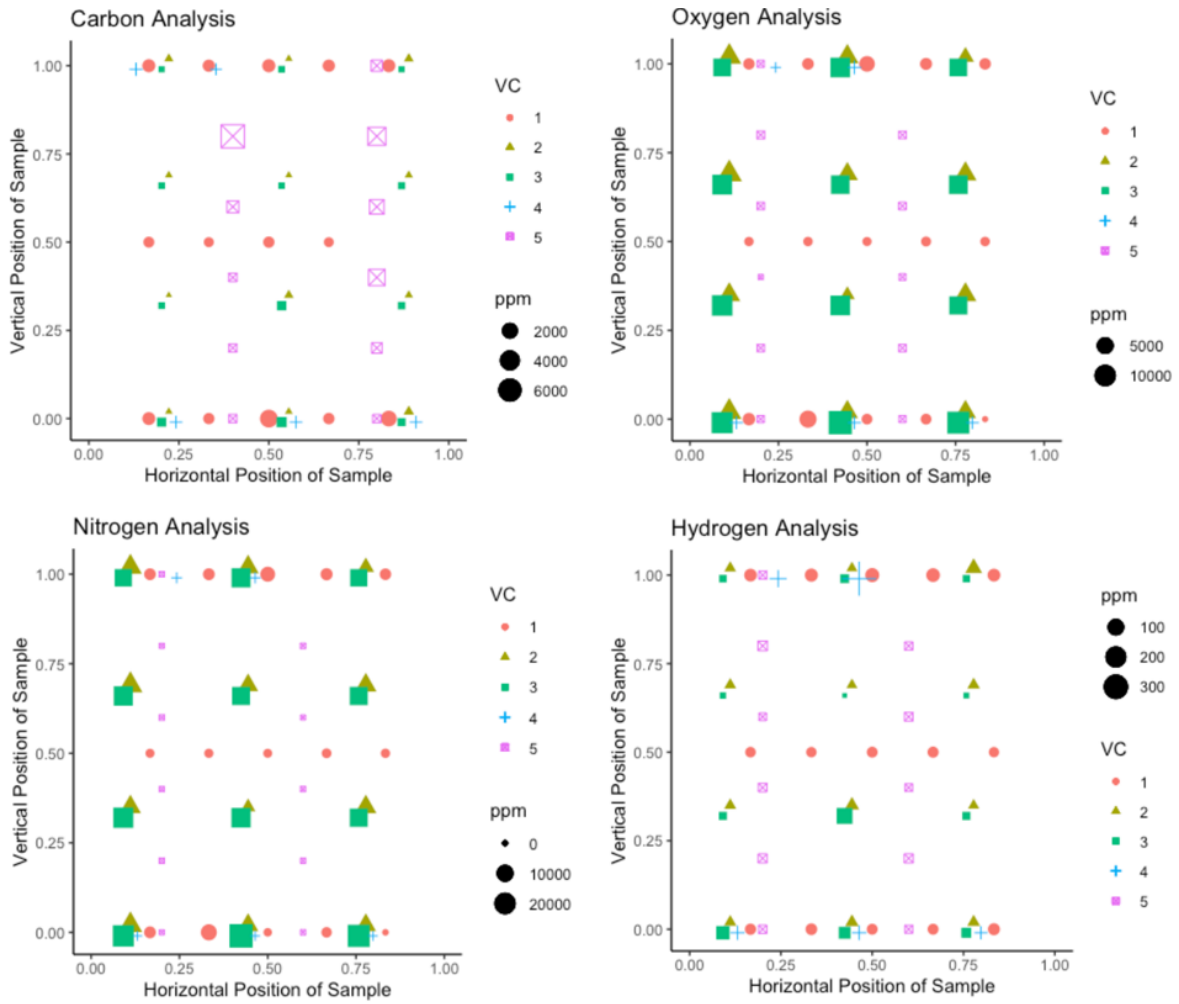

Figure 20: Visualization of the N (top left), O (top right), and C (bottom) contents across each casting related to position sample was taken from. The size of the symbol indicates the relative abundance with larger symbols correlating to higher impurity content.

5.0 Recommendations and Future Work

Five casting were carried out under the work scope. Two of these castings were successful using a novel inert TiC + Y_3O_2 coating and graphite crucible combination. Additional casting trials with this casting methodology are recommended to establish statistical significance, understand the success rate associated with these parameters, and optimize the method. Furthermore, future work should involve pouring the melt into a similarly coated mold to allow for a more practical final shape before further processing such as extrusion. In addition, the use of ZrO_2 crucibles or other ceramic crucibles of interest needs further investigation.

The use of VIM casting for highly reactive melts such as U-50Zr may not be the optimal choice. Cold hearth casting methods such as vacuum arc remelting and cold crucible suction casting may be more suited to further reduce contamination. This is evidenced by the lack of impurity addition as seen with the arc melting on a cold Cu hearth that made the master alloy for use in the VIM during these castings. These are mature technologies that could be incorporated in a manufacturing plant and potentially researched at scales such as the present work.

6.0 Conclusions

A methodology for successfully casting U-50Zr was sought in the present work. Previously reported works used small quantities of U-50Zr, whereas this work investigated a larger lab-scale quantity. The success was measured by ability to limit impurity elements such as C, O, N that result in carbide or α-phase stabilization as well as the UZr_2 phase purity of the sample. Five castings were carried out using arc melted master alloy feedstock. The methodologies used during arc melting and casting were coupled with analysis of the resulting C, O, N, H impurities, phase characterization and microscopy. This report summarizes the work carried out and ends with recommendations for a process to be more thoroughly investigated.

Multiple combinations of crucible and inert coating materials were investigated. Overall, the highest success castings were completed with a graphite crucible utilizing a TiC underlayer and Y_2O_3 overcoat in this work. Once proper coating procedures were established, this combination resulted in two successful castings. The two successful castings had C, O, and N contamination levels low enough that limited carbide and α-phase stabilization occurred while producing the desired δ-UZr_2 phase.

7.0 References

Ahn, S., Irukuvarghula, S., and McDeavitt, S. M., 2014, "Thermophysical Investigations of the Uranium–Zirconium Alloy System," Journal of Alloys and Compounds, **611**, pp. 355–362.

Bagchi, A. C., Prasad, G. J., Khan, K. B., and Singh, R. P., 2014, "A Study on Zirconium Rich Uranium–Zirconium Alloys," Trans Indian Inst Met, **67**(1), pp. 123–130.

Bagchi, A. C., Prasad, G. J., Khan, K. B., and Singh, R. P., 2014, "Study on Alloying Behaviour of Uranium Zirconium Alloy," Trans Indian Inst Met, **67**(3), pp. 443–449.

Basak, C., Prasad, G. J., Kamath, H. S., and Prabhu, N., 2009, "An Evaluation of the Properties of As-Cast U-Rich U–Zr Alloys," Journal of Alloys and Compounds, **480**(2), pp. 857–862.

Basak, C. B., Prabhu, N., and Krishnan, M., 2010, "On the Formation Mechanism of UZr2 Phase," Intermetallics, **18**(9), pp. 1707–1712.

Basak, C. B., Neogy, S., Srivastava, D., Dey, G. K., and Banerjee, S., 2011, "Disordered Bcc γ-Phase to δ-Phase Transformation in Zr-Rich U-Zr Alloy," Philosophical Magazine, **91**(24), pp. 3290–3306.

Ha, S.-J., Kuk, S.-W., Jeong, K.-C., Lee, Y.-K., and Park, J.-Y., 2021, "Potential Source of Carbon Contamination in U-Zr Melt Processed in Y2O3-Plasma-Spray-Coated Graphite," Journal of Nuclear Materials, **547**.

Huber, Z., McCoy, K. M., Athon, M., Schwerdt, I., and Lavender, C., 2021, "Effects of Casting Parameters and Impurity Concentrations on As-Cast U–10Mo," Progress in Nuclear Energy, **140**.

Huber, Z., Athon, M., Shen, S., Conte, E., McCoy, K., and Lavender, C., 2021, "Enhancing Isotope Mixing in U-10Mo Downblend Castings with Electromagnetic Stirring," Journal of Nuclear Materials, **555**.

Irukuvarghula, S., Ahn, S., and McDeavitt, S. M., 2016, "Decomposition of the γ Phase in As-Cast and Quenched U–Zr Alloys," Journal of Nuclear Materials, **473**, pp. 206–217.

Hofman, G. L., Pahl, R. G., Lahm, C. E., and Porter, D. L., 1990, "Swelling Behavior of U-Pu-Zr Fuel," MTA, 21(2), pp. 517–528.

Janney, D. E., 2018, *Metallic Fuels Handbook, Part 1: Alloys Based on U-Zr, Pu-Zr, U-Pu, or U-Pu-Zr, Including Those with Minor Actinides (Np, Am, Cm), Rare-Earth Elements (La, Ce, Pr, Nd, Gd), and Y*, INL/EXT-15-36520.

Khanolkar, A., Yao, T., Hua, Z., Dennett, C. A., Reese, S. J., Schley, R. S., He, L., Kennedy, J. R., and Hurley, D. H., 2021, "In Situ Monitoring of Microstructure Evolution during Thermal Processing of Uranium-Zirconium Alloys Using Laser-Generated Ultrasound," Journal of Nuclear Materials, **553**, p. 153005.

McCoy, K., Huber, Z., Athon, M., MacFarlan, P., and Lavender, C., 2020, *Thermomechanical Processing of Uranium Alloys with 10 and 50 Weight Percent Zirconium*, PNNL-30011.

Rough, F. A., Austin, A. E., Bauer, A. A., and Doig, J. R., 1956, The Stability and Existence Range of the Zirconium-Uranium Epsilon Phase, BMI-1092.

Pacific Northwest National Laboratory

902 Battelle Boulevard
P.O. Box 999
Richland, WA 99354

1-888-375-PNNL (7665)

www.pnnl.gov